Few-Shot Class-incremental SAR Target Recognition via Orthogonal Distributed Features

LINGZHE KONG
FEI GAO
XIAOYU HE
JUN WANG
JINPING SUN, Member, IEEE
Beihang University, Beijing, China

HUIYU ZHOU
University of Leicester, LE1 7RH Leicester, U.K.

AMIR HUSSAIN
Edinburgh Napier University, EH11 4BN Edinburgh, U.K.

***Abstract*—As synthetic aperture radar (SAR) imaging technology continues to evolve, the growing repository of SAR images depicting diverse types of observed targets has sparked rising interest in SAR target incremental recognition techniques. However, most existing SAR target incremental recognition algorithms typically require an ample amount of training data. In urgent scenarios such as emergency response and disaster relief, there may be a necessity to identify targets for which a substantial amount of data has not been previously accumulated. Algorithms designed for general scenarios often fail to achieve satisfactory performance in such situations. To tackle the aforementioned issues, this paper presents a few-shot incremental recognition algorithm for SAR targets based on orthogonal distributed features. Specifically, an orthogonal distribution optimization method for features is designed, which not only mitigates the feature confusion in few-shot incremental learning, but also reserves space for features of potential unseen classes. A random augmentation method for high-dimensional features is proposed to improve the overfitting problem while assisting in strengthening the boundaries between features of different classes. Furthermore, a joint decision criterion based on Euclidean distance and cosine distance is introduced, enabling the classifier to possess sufficient generalization ability and robustness in handling dynamic data. Experimental results on the MSTAR dataset show that the algorithm outlined in this paper outperforms existing methods in SAR target few-shot incremental recognition tasks, demonstrating its superior effectiveness.**

***Index Terms*—SAR automatic target recognition, Few-shot incremental learning, Orthogonal distribution, Random augmentation.**

This research was supported by the National Natural Science Foundation of China under Grant 62371022. *Corresponding authors: Fei Gao, and Xiaoyu He.*

Authors' addresses: Lingzhe Kong, Fei Gao, Xiaoyu He, Jun Wang and Jinping Sun are with the School of Electronic and Information Engineering, Beihang University, Beijing 100191, China (e-mail: klz1008@buaa.edu.cn; feigao2000@163.com; hexiaoyu@buaa.edu.cn; wangj203@buaa.edu.cn; sunjinping@buaa.edu.cn). Huiyu Zhou is with the Department of Informatics, University of Leicester, LE1 7RH Leicester, U.K. (e-mail: hz143@leicester.ac.uk). Amir Hussain is with the Centre of AI and Robotics, Edinburgh Napier University, EH11 4BN Edinburgh, U.K. (e-mail: a.hussain@napier.ac.uk).

I. INTRODUCTION

Target detection and recognition are pivotal in the intelligent interpretation of Synthetic Aperture Radar (SAR) images [1], [2]. Specifically, target recognition can provide crucial category information, holding significant value. Over recent years, convolutional Neural Network (CNN) based automatic target recognition (ATR) algorithms for SAR have showcased exceptional performance on numerous SAR datasets [3], [4], [5], [6]. However, conventional neural network models are designed for static tasks, which means they learn on fixed data to acquire recognition capabilities for the current task [7]. When faced with new tasks, they encounter "catastrophic forgetting," leading to a notable deterioration in classification performance for previously learned tasks [8], [9]. In real-world applications, the number of SAR targets to be recognized gradually accumulates, which necessitates the model to continually learn new classes while retaining recognition capabilities for old ones [10], [11]. To meet this practical demand, researchers are increasingly focusing on the field of incremental learning.

Incremental learning algorithms aim to facilitate models in continuously acquiring new knowledge while retaining previously attained knowledge. Initially, the neural network undergoes training on a base task with a certain set of classes to obtain a foundational model. Subsequently, new tasks, each including several new classes, arrive over time. As new tasks emerge, the model continually learns new knowledge, enabling it to identify an increasing number of classes. The main challenge faced by incremental learning is the stability-plasticity dilemma [12], [13]. Stability denotes the model's capacity to maintain previously acquired knowledge, while plasticity pertains to its ability to learn new knowledge. This dilemma implies that if the algorithm focuses on maintaining classification performance on old tasks, the model will struggle to adapt to new knowledge. Conversely, prioritizing the learning of new tasks may result in the model forgetting a significant amount of previously learned knowledge—both scenarios are unacceptable in incremental learning. Moreover, according to [14], inter-class confusion poses a significant challenge in SAR target incremental recognition. Images of the same target under different azimuth angles can vary significantly, while different targets under the same azimuth angle may appear more similar. Therefore, intra-class differences in SAR target images are relatively large, while inter-class differences are the opposite, making it easier for features of different classes to be confused in the feature space.

Currently, researchers have proposed SAR target incremental recognition algorithms from different perspectives to address the aforementioned issues [15], [16]. However, most existing SAR target incremental recognition algorithms are designed under the condition of abundant training data. In emergency scenarios such as disaster relief, it may be necessary to identify targets for which sufficient data has not been accumulated. In such cases, SAR target incremental recognition algorithms proposed for general situations often fail to achieve satisfactory performance, with a significant decrease in recognition accuracy. Therefore, studying SAR target incremental recognition algorithms tailored for few-shot conditions is of significant importance for better addressing complex real-world scenarios.

The general procedure of Few-Shot Class-Incremental Learning (FSCIL) is depicted in Fig. 1. The neural network is first trained on a foundational task with an ample number of samples to obtain the base model. Subsequently, few-shot tasks, each containing N classes with K samples, arrive sequentially over time. The model from the previous stage is used to initialize a new model. Then, the new model undergoes training with a few-shot incremental learning strategy to acquire recognition capabilities for the newly added classes, thus enabling continual learning under few-shot condition.

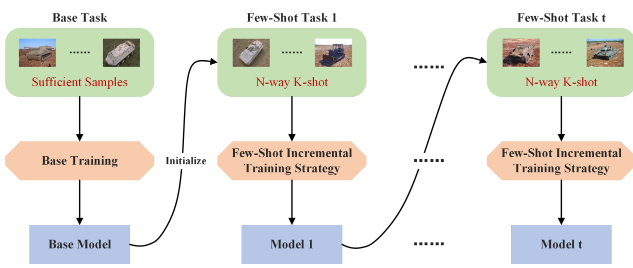

Fig. 1. The General Process of FSCIL

In the FSCIL task, the stability-plasticity dilemma becomes increasingly pronounced. The scarcity of samples increases the likelihood of neural network parameters overfitting during updates, thus diminishing the model's generalization ability, and compromising its stability. Conversely, freezing network parameters will lead to the model encountering difficulties in adapting to new classes, significantly reducing its plasticity [17], [18]. The few-shot new classes also results in a significant imbalance between the number of training samples available for base classes and those for new classes. Retraining the model with samples from both base and new classes introduces severe bias in classification. Moreover, due to constraints of data security or privacy, the training data of previously learned classes may not be accessible when the model learns new classes [12]. Therefore, retraining the model is not the most effective approach to address the continual emergence of new classes in FSCIL tasks. Additionally, under the few-shot condition, neural networks struggle to acquire sufficient knowledge to fully distinguish between different classes, further exacerbating feature confusion among various SAR targets. To tackle the stability-plasticity balance challenge and the feature confusion issue of similar classes in SAR target FSCIL tasks, we propose a few-shot incremental recognition algorithm for SAR targets, focusing on the feature distribution. The main contributions of this paper are outlined as follows:

(1) A feature space optimization process via orthogonal distribution is proposed, whereby features from various classes are constrained to predefined orthogonal directions, and intra-class differences are jointly reduced from both Euclidean and cosine distance perspectives. This approach not only effectively reduces mutual confusion among learned classes but also crucially reserves space for the incorporation of features from new classes.

(2) A high-dimensional feature random augmentation method is devised, wherein a series of pseudo-features is generated by applying random biases to real high-dimensional features. This method is employed to reinforce the representational capacity of real high-dimensional features for their respective classes under few-shot conditions, assisting in establishing more reliable classification boundaries among features of various classes.

II. RELATED WORKS

A. SAR Target Incremental Recognition

Recently, with the continuous development of SAR technology, there has been a steady increase in the number of high-resolution SAR images of various targets. This trend has imposed new demands on SAR ATR algorithms, namely, the ability to continuously learn new data. Motivated by the necessity to process dynamic data, researchers have shifted their focus towards SAR target incremental recognition.

Currently, the field of SAR target incremental recognition has seen some development, with researchers proposing various algorithms from perspectives such as data replay, regularization, and bias correction. From the data replay perspective, Dang et al. [16] proposed to select samples in intersecting and boundary regions as exemplars to enhance the recognition of easily confused samples. From the regularization perspective, Tang et al. [15] introduced a knowledge distillation technique leveraging models from several prior tasks, aimed at minimizing cumulative errors in incremental learning. Li et al. [14] utilized anchored feature centers in incremental learning process to reduce intra-class differences and increase inter-class differences, consequently aiding the model in discerning between new and previously learned classes. From the bias correction perspective, Huang et al. [19] advanced a memory-enhanced module to refine the network weights, which balances biases between new and old classes by extracting typical representations from the weights of old classes.

Although the aforementioned algorithms have demonstrated impressive performance in conventional SAR target incremental recognition tasks, the reality is that not all targets have an ample supply of training samples available. In certain urgent scenarios, such as emergency response and disaster relief, practical tasks may necessitate the identification of targets for which an adequate amount of data has not been accumulated. Therefore, the research on SAR target incremental recognition algorithms under few-shot conditions holds great significance for effectively addressing complex and diverse tasks.

B. Few-Shot Class-Incremental Learning

FSCIL is a focal point garnering attention from numerous researchers. It requires the model to continually learn new classes with a limited number of labeled samples while maintaining its classification capability for previously learned classes. Due to the insufficient training data, the stability-plasticity dilemma faced by conventional incremental learning becomes even more prominent under few-shot conditions, making the design of FSCIL algorithms highly challenging. Existing FSCIL algorithms are broadly classified into four categories: those based on replay mechanisms, weight regularization, dynamic network, and meta-learning techniques [18], [20].

Replay-based FSCIL algorithms typically store a few representative instances for each previously learned class. These examples are then employed to provide supervisory information for model updates, encompassing features of intermediate layers, output logits, and other relevant aspects [21]. For instance, Dong et al. [22] employed a knowledge distillation approach based on graph relation, maintaining a graph that expresses relationships between different classes to transfer previously learned knowledge. Cheraghian et al. [23] presented a semantic-aware knowledge distillation approach that incorporates semantic information from word embeddings to enhance the distillation process. Tai et al. [24] introduced a prototype distillation network, refining features and prototypes into a reduced-dimensional space to compress channels hindering the discrimination of different classes.

Weight regularization aims to control the updates of neural network parameters, preserving the model's classification capability for old classes by reducing deviations of important weights. Currently, researchers have proposed various weight-regularization-based FSCIL algorithms from different perspectives [25]. Shi et al. [26] struck an effective equilibrium between model stability and plasticity by designing a loss function that remains flat near the minimum, preventing model parameters from deviating from the optimal solution learned on old tasks. Zhou et al. [27] introduced a forward compatible FSCIL method that utilizes virtual prototypes to occupy part of the feature space during training. This method compresses the spatial distribution of learned classes, thereby enhancing the model's plasticity to accept subsequent updates. Zhao et al. [28] discovered that low-frequency components in the feature space are more important for retaining learned knowledge. Hence, discrete cosine transform is introduced to separate different frequency components of features, which reduces the mutual influence between knowledge of new and old classes. Akyürek et al. [29] proposed a subspace regularization method, constraining the weights of new classes to align closely with the subspace generated by the weights of old classes, thus better utilizing prior knowledge to distinguish between new and previously learned classes. Kim et al. [30] advanced a weight space rotation method, transforming the original model parameters into a new space and estimating the importance of different parameters to determine the flat direction in the loss function. The model is then fine-tuned along the flat direction to adapt to new classes.

The FSCIL algorithm based on dynamic networks automatically adjusts the network structure during the incremental learning process to better balance model stability and plasticity [31]. Specifically, Tao et al. [32] employed a neural gas network to maintain the spatial topological structure of old class features and address catastrophic forgetting in FSCIL tasks. Zhang et al. [33] introduced a graph attention network, treating the classifier weights as nodes in a graph. By aggregating information from different nodes and fusing it, the updated classification weights are obtained. This enables the classifier to continuously update its decision boundaries to adapt to new class features. Yang et al. [34] put forward a dynamic support network, initially expanding network nodes to accommodate knowledge from new classes, and then determining which expanded nodes to retain through a node self-activation mechanism. SoftNet, proposed by Yoon et al. [35], evaluates the importance of network parameters using a non-binary mask. During the incremental learning process, it freezes primary parameters while updating secondary parameters, effectively balancing catastrophic forgetting and overfitting issues.

Meta-learning aims to leverage existing knowledge to solve new problems [36]. During meta-training phase, models continuously learn how to recognize targets in few-shot scenarios by constructing multiple few-shot tasks. During meta-testing phase, novel samples are identified by forming few-shot incremental tasks similar to those encountered during training phase. Within the meta-learning framework, researchers have proposed various FSCIL algorithms. Zhu et al. [37] proposed a continual prototype learning strategy for FSCIL. On on hand, Random episode selection is used to enhance scalability by adapting feature representations to generated incremental episodes. On the other hand, dynamic relation projection is designed to calculate the prototypes' correlation matrix in a shared feature space for the self-promotion of prototypes. Hersche et al. [38] employed a meta-learning feature extractor with fixed parameters and trainable fully connected layers in the Constrained Few-shot Class-incremental Learning (C-FSCIL). They minimized the cosine similarity among prototypes through a nudging process and then fine-tuned the fully connected layers to align output features with nudged prototypes, facilitating feature separability among different classes.

Zou et al. [39] designed a margin-based FSCIL algorithm, which alleviates class-level overfitting issues by imposing additional constraints on margin-based patterns.

In the field of SAR ATR, research on few-shot target recognition for static tasks has been well-developed, with recent algorithms demonstrating excellent performance. For instance, Zhang and his team proposed two distinct few-shot recognition methods from the perspectives of azimuth-aware discriminative representation learning and domain knowledge-driven dual-stream network, both achieving high recognition accuracy [40], [41]. Yang et al. [42] presented a few-shot fine-grained classification method based on hierarchical embedding network and center calibration, which achieves high-precision recognition for targets from similar classes. Bai et al. [43] introduced an approach based on robust embedding and manifold inference, which fully exploits the information within high-dimensional features, thereby enabling accurate recognition. However, research on target recognition for dynamic tasks under few-shot conditions is relatively scarce. Existing work includes a cosine prototype learning framework proposed by Zhao et al. [18], an incremental evolutionary network with hierarchical embedding advanced by Wang et al. [17], and an azimuth-aware subspace classifier for FSCIL proposed by Zhao et al. [44]. Overall, the research on FSCIL for SAR images is still in its infancy, with the target recognition accuracy being relatively low. Many issues remain to be resolved.

III. METHODS

In this section, we first outline the problem setup of the FSCIL task. Then, we proceed to introduce our FSCIL methodology based on Orthogonal Distributed Features (ODF) by sequentially presenting the overall framework, algorithmic details, and implementation process.

A. Problem Setup

FSCIL aims to incrementally acquire knowledge from novel classes with only a limited number of labeled samples while maintaining the model's classification ability for previously learned classes. $\{T^0, T^1, \cdots, T^n\}$ represents incremental learning tasks at each stage, and $\{D^0, D^1, \cdots, D^n\}$ corresponds to the respective training set. $D^n = \{(x_i^n, y_i^n)\}_{i=1}^{|D^n|}$ includes $|D^n|$ training samples from task T^n, where x_i^n is a sample of class $y_i^n \in \mathbb{C}^n$, and $\mathbb{C}^n$ represents the classes encompassed within task T^n. It's important to note that classes from different tasks do not overlap, meaning that when $i \neq k$, $\mathbb{C}^i \cap \mathbb{C}^k = \phi$. The training set D^0 for the base task T^0 contains several classes, each with an ample amount of training samples, which are utilized to train the base model. The few-shot training set D^n for the incremental task $T^n\,(n \geq 1)$ is commonly described using N-way K-shot notation, which means D^n contains N classes, with each class having only K training samples. N is typically set to 1, 2, or 5, with a typical value for K being 5. In consideration of potential constraints on data security or data privacy in real-world application scenarios, the FSCIL process typically mandates the exclusion of complete data from previous tasks. Instead, only new class data, along with a minimal amount of old class exemplars as necessary, are permissible for learning. After the incremental training, the CNN model is evaluated using a test set containing all previously learned classes, i.e., $\mathbb{C}_{test}^n = \cup_{i=0}^n \mathbb{C}^i$.

B. Overall Framework

The diagram of ODF proposed in this paper is depicted in Fig. 2. Incremental learning tasks arrive continuously over time. The base task comprises several classes with an ample number of training instances, whereas every incremental task comprises N classes, each with only K training samples. SAR images are input into the neural network model f_θ to obtain features and classification predictions. f_θ consists of a feature extractor f_φ and a dimensionality reduction layer σ. Specifically, f_φ represents a ResNet-18 model [45], utilized for mapping input images to high-dimensional features of 512 dimensions. σ denotes a fully connected layer responsible for reducing the dimensionality of the 512-dimensional features to 64 dimensions, aiming to eliminate redundant information within the features.

In the FSCIL process, an orthogonal distribution optimization method for features and a random augmentation method for high-dimensional features are employed to optimize the model. Before training begins, a set of orthogonal vectors is established in the feature space to reserve positions for all potential classes. During the base training stage, prototypes of all base classes are assigned to predefined orthogonal directions, and intra-class differences in features are reduced from both Euclidean and cosine distance perspectives. After base training, prototypes of base classes and a small subset of high-dimensional features are preserved. During the incremental learning stage, parameters of the feature extractor are frozen while the dimensionality reduction layer remains trainable. High-dimensional features of new class images are extracted by the feature extractor and merged with high-dimensional features preserved in all previous stages. Subsequently, the parameters of the dimensionality reduction layer are updated to allocate prototypes for new classes onto unused orthogonal directions, while minimizing the offset of prototypes from the old classes as much as possible. Additionally, random bias is applied to each preserved high-dimensional feature to perform random augmentation, generating pseudo high-dimensional features of both old and new classes to collectively update parameters of the dimensionality reduction layer along with real high-dimensional features. When calculating classification confidences, predictions derived from Euclidean distance criterion and cosine distance criterion are fused to enhance the generalization and robustness of the classifier, rendering the calculation of classification confidences for few-shot incremental recognition more

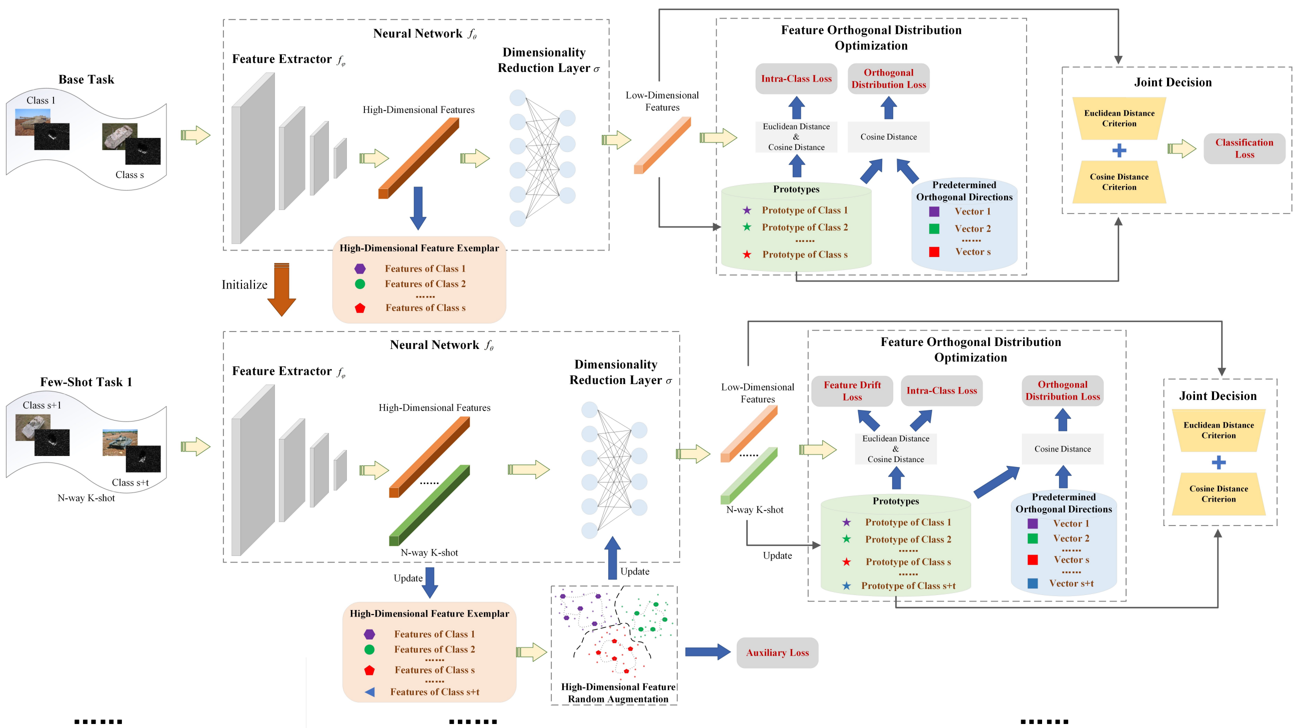

Fig. 2. The Framework of ODF Algorithm

rational. The principles and effects of the aforementioned methods are elaborated in Sections III-C, III-D, and III-E, while the implementation details of ODF are outlined in Section III-F.

C. Feature Orthogonal Distribution Optimization

In FSCIL tasks, the neural network model maps input images of different classes to discriminable features in feature space to distinguish between different classes. Therefore, the spatial distribution of features is an important factor influencing recognition results. If the prototypes of new classes resemble those of previously learned classes, distinguishing between samples from these classes becomes challenging. Some existing FSCIL algorithms propose continuously adjusting prototypes during the incremental learning to increase the distance between prototypes of different classes. However, such prototype fine-tuning necessitates simultaneous consideration of the positional relationships between the prototypes of the new class and all previously learned classes. When the task involves multiple new classes, consideration of the relative positions of different new class prototypes is also necessary. Excessive influencing factors make it difficult to strike a balance between a sufficiently large spatial distance among prototypes and leaving room to accommodate the new classes. Therefore, the model's stability and plasticity fail to achieve a satisfactory equilibrium.

To achieve a more reasonable feature space distribution in the SAR target few-shot incremental recognition task, this paper proposes an orthogonal distribution optimization method for features. As depicted in Fig. 3, the feature orthogonal distribution optimization method first allocates prototypes of different classes to predefined orthogonal directions. Subsequently, it reduces the distance between features and their respective prototypes, thereby approximating orthogonality among features of different classes overall. Considering the feature drift caused by model updates in the FSCIL process, as well as the large intra-class differences in SAR images, constraints based on a single distance criterion struggle to maintain the orthogonality of features. Therefore, we simultaneously employ Euclidean distance and cosine distance to obtain stronger constraints on the intra-class distribution of features. The feature orthogonal distribution optimization, through the orthogonal constraint of inter-class distribution and the dual-distance criterion constraint of intra-class distribution, not only reduces inter-class feature confusion but also endows features of different classes with good separability under both the cosine distance and Euclidean distance, which are commonly used classification criteria in few-shot learning. More importantly, the unallocated target directions reserve sufficient space for potential new classes, thereby facilitating the model's adaptation to new class knowledge. Ultimately, the model achieves a better balance between stability and plasticity under few-shot conditions.

Based on the above analysis, the specific implementation of feature orthogonal distribution optimization is described as follows. Before the start of incremental learning, a set of orthogonal vectors $\{o_1, o_2, \cdots, o_m\}$ is predefined according to the dimension of output features of the dimensionality reduction layer, where m represents

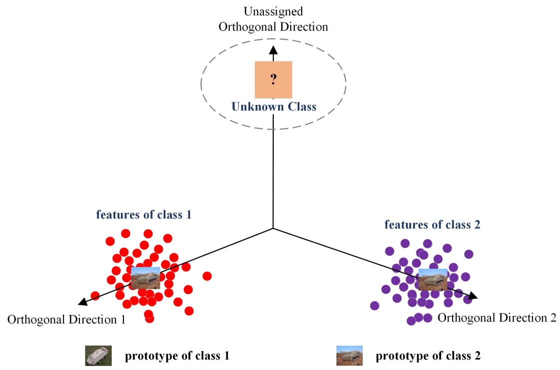

Fig. 3. Schematic Diagram of the Orthogonal Distribution Optimization Method for Features

the total number of classes that may emerge during the incremental learning process. These predefined vectors help delineate target directions in the feature space. In the base training stage, the base task consists of N classes, and prototypes of these classes will be assigned to the target directions delineated by the orthogonal vectors $\{o_1, \cdots, o_N\}$. For any class $k\,(k = 1, 2, \cdots, N)$ in the base training set, the training samples are denoted as $D_k^0 = \left\{\left(x_{i_k}^0, y_{i_k}^0\right)\right\}_{i_k=1}^{|D_k^0|}$. To align the base training process with the incremental training process, episodic training is employed during base training to simulate the few-shot condition encountered in incremental training. In each training epoch, S samples are randomly drawn from D_k^0 to construct a support set $\left\{\left(x_{i_s}^0, y_{i_s}^0\right)\right\}_{i_s=1}^{S}$, and Q samples are randomly sampled from D_k^0 to form a query set $\left\{\left(x_{i_q}^0, y_{i_q}^0\right)\right\}_{i_q=1}^{Q}$. Initially, the neural network f_θ extracts features from samples in both the support set and the query set. The prototype p_k is derived by calculating the average of the support set features:

$$p_k = \frac{1}{S}\sum_{i_s=1}^{S} f_\theta\left(x_{i_s}^0\right) \tag{1}$$

The cosine distance between p_k and its corresponding orthogonal vector o_k is calculated, serving as the orthogonal distribution loss:

$$L_{orthogonal} = \sum_{k=1}^{N} d_{\cos}\left(\frac{p_k}{|p_k|}, \frac{o_k}{|o_k|}\right) \tag{2}$$

Here, $d_{\cos}(\cdot)$ represents the cosine distance. Subsequently, the intra-class loss of features is jointly calculated from both the Euclidean distance and cosine distance aspects using the query set features of each class and the prototypes:

$$\begin{aligned} L_{intra} &= \alpha \cdot \frac{1}{Q}\sum_{k=1}^{N}\sum_{i_q=1}^{Q}\left(f_\theta\left(x_{i_q}^0\right) - p_k\right)^2 \\ &+ \frac{1}{Q}\sum_{k=1}^{N}\sum_{i_q=1}^{Q} d_{\cos}\left(\frac{f_\theta\left(x_{i_q}^0\right)}{\left|f_\theta\left(x_{i_q}^0\right)\right|}, \frac{p_k}{|p_k|}\right) \end{aligned} \tag{3}$$

As a scale factor, α is used to balance the constraints of Euclidean distance and cosine distance. Finally, the cross-entropy loss is calculated using the classification predictions of the query set samples and their corresponding labels as the classification loss L_{cls}. Combining the three aforementioned losses, the total loss for the base training is calculated as:

$$L_{base} = \beta L_{cls} + \gamma L_{orthogonal} + L_{intra} \tag{4}$$

β and γ are hyperparameters used to regulate the strength of the constraints for L_{cls} and $L_{orthogonal}$. After base training, the prototypes for all classes are saved. Simultaneously, S support set samples for each class are input into the feature extractor f_φ, yielding corresponding S high-dimensional features, which are then saved.

When the model learns the incremental task $T^n\,(n \geq 1)$, the feature extractor f_φ is frozen, while the parameters of the dimensionality reduction layer σ remain trainable. Assuming the number of previously learned classes is M^n and the number of classes in T^n is C^n, the predefined first M^n target directions have already been allocated. The prototypes of the new classes will be assigned to the target directions corresponding to the orthogonal vectors $\{o_{M^n+1}, \cdots, o_{M^n+C^n}\}$. For the $k\,(k = 1, 2, \cdots, C^n)$th new class in the incremental dataset, the training samples are represented by $D_k^n = \left\{\left(x_{i_k}^n, y_{i_k}^n\right)\right\}_{i_k=1}^{|D_k^n|}$. The training samples of each class are first input into the feature extractor to obtain high-dimensional features:

$$\varepsilon_{i_k}^{c_{new}} = f_\varphi\left(x_{i_k}^n\right) \tag{5}$$

Next, the high-dimensional features of the new classes are merged with those of the old classes $\varepsilon^{c_{old}}$ to update the saved high-dimensional feature set:

$$\varepsilon^c = \varepsilon^{c_{new}} \cup \varepsilon^{c_{old}} \tag{6}$$

Finally, all features from the updated high-dimensional feature set are simultaneously fed into the dimensionality reduction layer to calculate low-dimensional features. For the new classes, the low-dimensional features are used to compute the prototypes through mean calculation, which, along with the corresponding orthogonal vectors, are used to compute the orthogonal distribution loss $L_{orthogonal}$ according to Eq. 2. Simultaneously, the intra-class loss L_{intra} is calculated using Eq. 3 with the low-dimensional features of the new classes and their corresponding prototypes to reduce intra-class differences. For the old classes, with the aim of mitigating the prototype drift caused by parameter updates to the dimensionality reduction layer, the weighted sum of Euclidean distance and cosine distance between the prototypes before and after the updates are used as the feature drift loss for the old classes:

$$L_{drift} = \alpha \sum_{k=1}^{M^n} ({p'}_k - p_k)^2 + \sum_{k=1}^{M^n} d_{\cos}\left(\frac{{p'}_k}{|{p'}_k|}, \frac{p_k}{|p_k|}\right) \quad (7)$$

α is a scale factor to balance the constraints of Euclidean distance and cosine distance. p_k represents the prototypes of old classes before the update of the dimensionality reduction layer, and p'_k represents the prototypes of old classes after the update of the dimensionality reduction layer. In summary, the total loss during the incremental training stage is depicted as follows:

$$L_{inremental} = \gamma L_{orthogonal} + L_{intra} + L_{drift} \quad (8)$$

In the process of feature orthogonal distribution optimization, it is evident that only the disparity between prototypes and the target directions, along with the intra-class differences of features, need to be considered. There's no longer a need to simultaneously calculate the positional relationships between all prototypes. This effectively reduces the factors affecting prototype adjustments, making model fine-tuning more conducive to convergence.

D. Random Augmentation of High-Dimensional Features

During the FSCIL process, with only a limited quantity of saved samples from previously learned classes and data from new classes available for model updates, the model not only encounters severe feature confusion but is also highly prone to overfitting. In order to further ameliorate the negative impact caused by the few-shot condition on recognition and to help maintain the orthogonality of features, a random augmentation method for high-dimensional features is presented in this paper.

Fig. 4 illustrates the concept of high-dimensional feature random augmentation. Due to the constraint of few-shot condition, during the parameter updates of the dimensionality reduction layer in the incremental learning stage, there are only a few high-dimensional features available for both new and old classes. Random augmentation introduces several pseudo high-dimensional features that possess certain representational capabilities for their respective classes by applying random biases to these real high-dimensional features. The effect of this process is directly evident in the expansion of the spatial distribution characterized by real high-dimensional features for each class. For both the base and new classes, the limited number of real high-dimensional features can only represent a small subset of the entire feature space occupied by the corresponding class. This makes it difficult for the model to map all high-dimensional features of the same class to the preset orthogonal directions, thereby affecting the final classification results. The presence of pseudo high-dimensional features expands the class boundaries, simulating the features of some same-class samples that differ significantly from the real high-dimensional features. This allows more high-dimensional features to be correctly mapped to the preset orthogonal directions. Hence, updating the model parameters using both real and pseudo high-dimensional features not only assists in distinguishing features of different classes but also enriches the training data, thereby alleviating the overfitting issue.

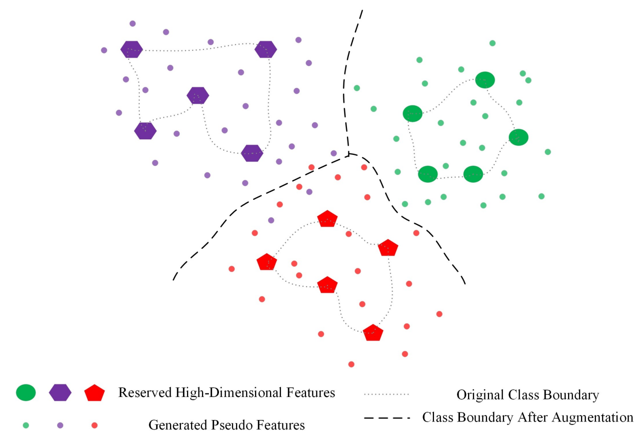

Fig. 4. Schematic Diagram of High-Dimensional Feature Random Augmentation

Based on the aforementioned analysis, the specific implementation of high-dimensional feature random augmentation is described as follows. When the model learns task $T^n\,(n \geq 1)$, the training samples of the new classes are denoted as $D^n = \{(x_i^n, y_i^n)\}_{i=1}^{|D^n|}$, and the feature extractor with frozen parameters is denoted as f_φ. The high-dimensional features for the new classes $\varepsilon^{c_{new}}$ can be computed using Eq. 5. The saved high-dimensional features of the learned classes are denoted as $\varepsilon^{c_{old}}$. By merging the high-dimensional features of both new and old classes, we obtain an updated set of high-dimensional features, denoted as ε^c. Random bias following a standard Gaussian distribution is added to each sample in the high-dimensional feature set, thereby generating several pseudo high-dimensional features centered around each sample:

$$\mu_i^{\varepsilon_j^c} = \varepsilon_j^c + e_i * r \quad (9)$$

$\mu_i^{\varepsilon_j^c}$ represents the i-th pseudo high-dimensional feature generated by applying Gaussian random bias e_i around the j-th sample in the high-dimensional feature set. r serves as the scale factor of the bias, allowing control the dispersion range of pseudo high-dimensional features around the real ones. The label of $\mu_i^{\varepsilon_j^c}$, denoted as $y_i^{\varepsilon_j^c}$, is identical to that of ε_j^c. All generated pseudo high-dimensional features are fed into the dimensionality reduction layer σ to compute pseudo low-dimensional features. Then, the classification confidence P is computed for all pseudo low-dimensional features with respect to the prototypes of each class. Finally, cross-entropy loss is computed as an auxiliary loss using the classification confidence of pseudo low-dimensional features and their corresponding labels:

$$L_{auxiliary} = -\sum y_i^{\varepsilon_j^c} \log(P) \tag{10}$$

After incorporating the auxiliary loss, the total loss function during the incremental training process will be rewritten as:

$$L'_{incremental} = \gamma L_{orthogonal} + L_{intra} + L_{drift} + L_{auxiliary} \tag{11}$$

E. Joint Decision Criterion

In the FSCIL process, the classifier not only needs to effectively distinguish features of new classes in the current task but also needs to differentiate between features of new and old classes from different tasks, which presents challenges to the classifier's robustness and its generalization capability. Research in reference [17] has demonstrated that a classifier combining Euclidean and cosine distances can effectively enhance classification performance. In the orthogonal distribution optimization process proposed in this paper, features from different classes are assigned to a set of mutually orthogonal directions. Additionally, the intra-class Euclidean distance and cosine distance are minimized. This ensures that different classes exhibit good separability under both Euclidean and cosine distance criteria. Considering the well-matched feature distribution resulting from orthogonal optimization and the joint distance classifier, we also adopt a joint decision criterion based on Euclidean and cosine distances. It effectively utilizes the characteristics of orthogonal feature distribution to enhance the incremental recognition performance in few-shot scenarios.

After learning the task T^n, the neural network model is represented by f_θ, and the overall count of previously learned classes is C. The test set for this stage is denoted as $\mathbb{Q} = \{(x_i, y_i)\}_i^{N_n}$, where $y_i \in \cup_{k=0}^{n} \mathbb{C}^k$ corresponds to the labels. The prototypes $p_c \left(c \in \cup_{k=0}^{n} \mathbb{C}^k\right)$ of each class are calculated using Eq. 1. With reference to the Euclidean and cosine distances between the features and the prototypes, the classification output of any test sample can be computed under two different criteria, respectively:

$$P_{Euc}\left({y'}_i = c|x_i\right) = \frac{\left[1 + d_{Euc}\left(f_\theta\left(x_i\right), p_c\right)\right]^{-1}}{\sum_c^C \left[1 + d_{Euc}\left(f_\theta\left(x_i\right), p_c\right)\right]^{-1}} \tag{12}$$

$$P_{\text{Cos}}\left({y'}_i = c|x_i\right) = \frac{\left[1 + d_{\cos}\left(f_\theta\left(x_i\right), p_c\right)\right]^{-1}}{\sum_c^C \left[1 + d_{\cos}\left(f_\theta\left(x_i\right), p_c\right)\right]^{-1}} \tag{13}$$

Here, $P_{Euc}\left({y'}_i = c|x_i\right)$ and $P_{\text{Cos}}\left({y'}_i = c|x_i\right)$ respectively represent the confidence of sample x_i belonging to class c under the Euclidean distance criterion and the cosine distance criterion. $d_{Euc}(\cdot)$ and $d_{cos}(\cdot)$ stand for Euclidean distance and cosine distance.

Subsequently, these two confidences are combined into a joint decision confidence through the weighted sum with adaptive coefficients:

$$\begin{aligned} P_{total}\left({y'}_i = c|x_i\right) = a \cdot P_{\text{Cos}}\left({y'}_i = c|x_i\right) \\ +b \cdot P_{Euc}\left({y'}_i = c|x_i\right) \end{aligned} \tag{14}$$

Wherein, a represents the weighted coefficient of the confidence calculated based on the cosine distance criterion, while b denotes the weighted coefficient of the confidence calculated based on the Euclidean distance criterion. They automatically adjust during the decision-making process to better combine the decisions made based on the two criteria. The computation of a and b is illustrated in Eq. 15 and Eq. 16:

$$a = \frac{\max\left(P_{Cos}\left({y'}_i = c|x_i\right)\right)}{\max\left(P_{Cos}\left({y'}_i = c|x_i\right)\right) + \max\left(P_{Euc}\left({y'}_i = c|x_i\right)\right)} \tag{15}$$

$$b = \frac{\max\left(P_{Euc}\left({y'}_i = c|x_i\right)\right)}{\max\left(P_{\text{Cos}}\left({y'}_i = c|x_i\right)\right) + \max\left(P_{Euc}\left({y'}_i = c|x_i\right)\right)} \tag{16}$$

$\max\left(P_{\text{Cos}}\left({y'}_i = c|x_i\right)\right)$ and $\max\left(P_{Euc}\left({y'}_i = c|x_i\right)\right)$ respectively represent the maximum values of the classification confidences based on the cosine distance criterion and the Euclidean distance criterion. It can be observed that the joint decision confidence will lean towards the criterion that can make a clear judgment (i.e., where the confidence for a particular class significantly surpasses that of other classes, rather than having similar confidences for multiple classes). It assigns greater weight to such criterion and takes into account the decision of the other criterion appropriately, thereby minimizing the chances of the classifier providing a classification result when it cannot make an accurate judgment.

Finally, the class corresponding to the maximum value in the joint decision confidence is taken as the classification result:

$$y_{prediction} = \underset{c \in \{1, \cdots, C\}}{\arg\max} \left(P_{total}\right) \tag{17}$$

This classification result is derived from the spatial relationships between the features and the prototypes measured by Euclidean distance and cosine distance. It aligns with the distribution characteristics of features optimized by orthogonal distribution, hence offering a more accurate classification compared to results based on a single criterion.

F. Algorithm Implementation

The proposed ODF algorithm improves SAR target incremental recognition performance under the few-shot condition by employing feature orthogonal distribution optimization, high-dimensional feature random augmentation, and joint decision criterion. The implementation details of ODF are shown in Algorithm 1.

Algorithm 1: Implementation Process of ODF.

Input: A series of labeled data $D^0, D^1, \cdots, D^n$
Output: A trained CNN model f_θ

```
// Base Session with D^0
for epoch in epochs: do
    Construct a support set and a query set;
    Calculate protypes with support set features;
    Calculate L_orthogonal, L_intra and L_cls;
    The total loss for the base session is:
    L_base = βL_cls + γL_orthogonal + L_intra;
end
Construct high-dimensional feature exemplar ε^c;
Construct prototype set {p_k};
// Incremental Session with D^k (k ≥ 1)
for k ← 1 to n do
    Extract new-class features and update
      high-dimensional feature exemplar ε^c;
    Generate pseudo high-dimensional features;
    for epoch in inremental epochs do
        Calculate L_orthogonal, L_intra, L_drift,
          L_auxiliary;
        The total loss for incremental sessions is:
        L'_incremental =
          γL_orthogonal + L_intra + L_drift + L_auxiliary;
    end
    Update prototype set {p_k}
end
```

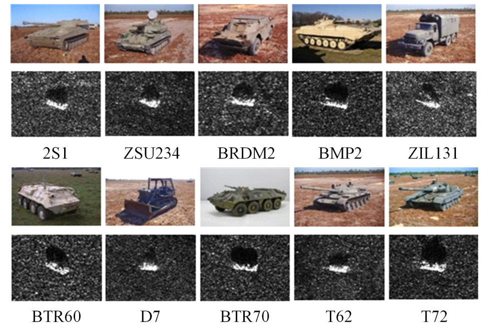

Fig. 5. Example of optical and SAR images in MSTAR dataset

TABLE I
Statistical Information of the MSTAR dataset

Targets	Training Samples(17°)	Testing Samples(15°)
D7	299	274
BMP2	233	195
ZSU234	299	274
BTR70	233	196
ZIL131	299	274
BTR60	256	195
2S1	299	274
BRDM2	298	274
T62	299	273
T72	299	274
Total	**2747**	**2425**

IV. EXPERIMENTS

A. Experimental Settings

To assess the effectiveness of the proposed ODF approach for SAR target few-shot incremental recognition tasks, various experiments are conducted based on the MSTAR dataset. The experimental results are compared with several FSCIL algorithms.

The MSTAR dataset originates from the Moving and Stationary Target Acquisition and Recognition Program, a collaboration between the Defense Advanced Research Projects Agency (DARPA) and the Air Force Research Laboratory. [46]. This dataset is compiled using high-resolution synthetic aperture radar operating in the X-band, featuring a resolution of 0.3m × 0.3m and HH polarization. It comprises SAR images of 10 types of ground mobile targets across various azimuth angles, observed under two elevation angles: 15° and 17°. Typically, images with an elevation angle of 17° are allocated for training, while those taken at 15° elevation angle are reserved for testing. The optical and SAR images for each target are shown in Fig. 5. The detailed statistics of the dataset are shown in Table I.

The FSCIL experiments are conducted in three different scenarios: 1-way 5-shot, 2-way 5-shot, and 1-step 5-shot. In the 1-way 5-shot scenario, the model initially learns four classes with sufficient samples, and in each incremental stage, learns one new class with only five samples. In the 2-way 5-shot scenario, the model initially learns four classes with sufficient samples, and in each incremental stage, learns two new classes, each with five samples. In the 1-step 5-shot scenario, the model initially learns five classes with sufficient samples, and in the incremental learning stage, learns the remaining five classes, with each class having only five training samples. The task division for model training in these three scenarios is outlined in Table II.

TABLE II
Task Division for Incremental Learning.

Target Type	Task Division		
	1-way 5-shot	2-way 5-shot	1-step 5-shot
2S1	T^0	T^0	T^0
BMP2			
BRDM			
BTR70			
BTR60	T^1	T^1	
D7	T^2		T^1
T62	T^3	T^2	
T72	T^4		
ZIL131	T^5	T^3	
ZSU234	T^6		

The ODF method is implemented in the PyTorch framework [47], and the model is trained with the Adam optimizer. The base training process encompassing 2000 epochs, with an initial learning rate configured to 0.01. The learning rate undergoes a tenfold decrement at epoch 1250, 1500, and 1750, respectively. During the incremen-

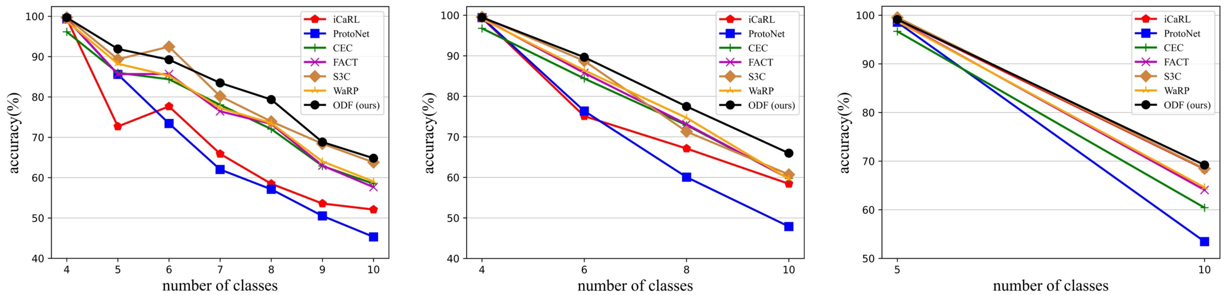

(a) (b) (c)

Fig. 6. Accuracy Curves for Three Different Scenarios. (a) 1-way 5-shot scenario. (b) 2-way 5-shot scenario. (c) 1-step 5-shot scenario.

tal learning stage, the feature extractor is frozen, leaving the parameters of the dimensionality reduction layer trainable. The incremental training comprises 200 epochs, with an initial learning rate of 0.1. The learning rate decreases tenfold at epoch 100, 150, and 175. The hyperparameters α and β in the loss function are configured to 0.001 and 0.2, while γ is set to 20 for base training and 3 for incremental learning. The number of pseudo-features generated around each real high-dimensional feature is set to 10, and the scale factor r for the random bias is set to 2.5.

B. Few-Shot Incremental Recognition Results

To illustrate the advantages of the algorithm introduced in this paper, we conducted incremental recognition performance comparisons under few-shot conditions using ODF against various algorithms. The compared algorithms include Incremental Classifier and Representation Learning (iCaRL) [48], Prototypical Networks for Few-shot Learning (ProtoNet) [49], Few Shot Incremental Learning with Continually Evolved Classifiers (CEC) [33], C-FSCIL [38], Forward Compatible Few-Shot Class-Incremental Learning (FACT) [27], Self-Supervised Stochastic Classifiers for Few-Shot Class-Incremental Learning (S3C) [50], and Warping the space: Weight space rotation for class-incremental few-shot learning (WaRP) [30]. Specifically, iCaRL is a classic incremental learning algorithm, ProtoNet is a typical few-shot learning network, and CEC, C-FSCIL, FACT, S3C, and WaRP are all recently proposed algorithms for FSCIL. All these algorithms are implemented based on ResNet-18 [45] to ensure the fairness of the comparative experiments.

As depicted in Fig. 6, subplots (a), (b), and (c) respectively delineate the trends in fluctuation of target recognition accuracy for both the proposed ODF and comparative algorithms across three different FSCIL scenarios. In each of the three scenarios, all algorithms demonstrate notable success in achieving high recognition accuracy in the base task. However, in the subsequent stages, as the total number of classes increases and there is a scarcity of training samples for both previously learned and newly introduced classes, the model experiences a gradual decline in recognition accuracy.

Compared to the comparative algorithms, ODF exhibits a slower decline in recognition accuracy, yielding superior target recognition performance. iCaRL is designed for conventional incremental learning scenarios, relying on a sufficient amount of data, thus exhibiting unstable recognition performance in few-shot scenarios. While ProtoNet is designed for few-shot recognition tasks, it lacks appropriate parameter update methods for incremental learning, resulting in limited model plasticity to continuously emerging new classes. For the comparative FSCIL algorithms, they lack sufficient consideration for the characteristics of SAR images. The distinctive attributes of SAR images in neural network models primarily manifest in the fact that the imaging results of the same target under different azimuth angles are not consistent, while different targets under the same azimuth angle may appear similar. Consequently, SAR images contain complex information with large variations within classes and small disparities between classes. The nudging process adopted by C-FSCIL struggles to impart sufficient discriminability to features of different classes in face of more challenging feature space distributions, leading to significant feature confusion in certain classes. FACT compresses the feature space of learned classes using pseudo prototypes to reserve space for potential new class features. However, the inadequate representation capability of virtual features for SAR image features leads to a mismatch between the reserved space and the features of new classes, which limits the model's capability of adapting to new classes. CEC utilizes a graph neural network to aggregate and integrate information from prototypes of different classes, but the complexity of SAR image information results in the inclusion of some irrelevant or redundant information, thereby limiting the improvement of classification performance. Furthermore, the complexity of SAR images makes it difficult for WaRP to find suitable flat directions, thus failing to effectively avoid the mutual influence between old and new classes.

In contrast, ODF directly focuses on the characteristics of large variations within classes and small disparities between classes in SAR images. By allocating features of different classes to orthogonal directions, it not only reduces mutual interference between new and old classes but also reserves space for new classes in advance. Additionally, random augmentation of high-dimensional features supplements information for the accurate recognition of each class and effectively alleviates overfitting issues. The joint decision based on Euclidean distance and cosine distance comprehensively considers the classification confidence under both criteria, leading to more reasonable classification results. Ultimately, ODF achieves high target recognition accuracy across different scenarios.

Table III, IV and V further present metrics including recognition accuracy, average accuracy, and Performance Drop rate (PD rate) [33] of each algorithm in the 1-way 5-shot, 2-way 5-shot, and 1-step 5-shot scenarios. In these tables, we denote the optimal values in bold and the suboptimal values with an underline. The algorithm advanced in this paper consistently demonstrates superior performance with the highest average accuracy and the lowest PD rate across all three scenarios, indicating that ODF not only outperforms the comparative algorithms in intermediate stages of incremental learning but also better balances the classification knowledge of both new and old classes after learning all classes.

Furthermore, it's worth noting that ODF demonstrates higher adaptability to different incremental learning scenarios. In general, the more incremental learning stages there are, the lower the average recognition accuracy tends to be, making it increasingly challenging to strike a balance between the model's stability and plasticity. ODF achieves an average recognition accuracy of 84.17%, with a PD rate of 29.93% in the 1-step 5-shot scenario. When the scenario changes to 2-way 5-shot, the average recognition accuracy of ODF only decreases by about 1%, with a 3.57% increase in PD rate. In the 1-way 5-shot scenario, the target recognition accuracy and PD rate of ODF are similar to those in the 2-way 5-shot scenario. On the contrary, among all comparative algorithms, iCaRL achieves similar recognition accuracy to ODF in the 1-step 5-shot scenario, but when the scenario changes to 2-way 5-shot and 1-way 5-shot, its target recognition performance decreases significantly, lagging behind ODF by around 10%. S3C achieves recognition accuracy similar to ODF in the 1-step 5-shot and 1-way 5-shot scenarios, but its target recognition performance exhibits significant fluctuations in the 2-way 5-shot scenario. Other algorithms such as WaRP and FACT exhibit similar fluctuation trends in average recognition accuracy and PD rate to ODF in different scenarios but fail to achieve recognition performance similar to ODF in any scenario. Obviously, the algorithm introduced in this paper exhibits enhanced adaptability to various few-shot incremental recognition scenarios, which is more in line with practical application requirements.

C. Ablation Experiments

This paper leverages orthogonal distribution optimization, high-dimensional feature random augmentation, and joint decision with Euclidean and cosine distance simultaneously to improve few-shot incremental recognition performance for SAR targets. To comprehensively assess the effectiveness of aforementioned methods, various ablation experiments are conducted in the 1-way 5-shot, 2-way 5-shot, and 1-step 5-shot scenarios.

Tables VI and VII present the incremental recognition accuracy of the model under two conditions: first, using samples from both previously learned and new classes for parameter fine-tuning, and second, feature orthogonal distribution optimization. It can be observed that feature orthogonal distribution optimization effectively improves recognition accuracy at various stages of incremental learning across different scenarios. In the 1-way 5-shot, 2-way 5-shot, and 1-step 5-shot scenarios, after the model has learned targets of all 10 classes, the recognition accuracy using feature orthogonal distribution optimization increases by 14.36%, 9.59%, and 12.01%, respectively, compared to using parameter fine-tuning. This result demonstrates the effectiveness of feature orthogonal distribution optimization in enhancing the model's performance in few-shot incremental recognition.

To better illustrate the impact of the orthogonal distribution optimization on the spatial distribution of features, we further provide visualizations of t-distributed Stochastic Neighbor Embedding (t-SNE) [51] for features extracted from the test set under three scenarios, when using parameter fine-tuning and feature orthogonal distribution optimization. In Fig. 7, subplots (a), (b), and (c) correspond to the 1-way 5-shot, 2-way 5-shot, and 1-step 5-shot scenarios respectively. Compared to parameter fine-tuning, feature orthogonal distribution optimization effectively reduces feature confusion between different classes. For example, when using parameter fine-tuning in the 1-way 5-shot scenario, significant confusion is observed among features corresponding to D7, T62, ZSU234, and ZIL131. The overlap of features is so severe that features corresponding to D7 are almost indistinguishable. As a result, there is almost no discriminability among these classes. Furthermore, there is varying degrees of confusion observed between features of 2S1 and T72, T72 and BMP2, BRDM2 and some other classes. This explains why parameter fine-tuning struggles to perform well in few-shot incremental recognition tasks. When employing feature orthogonal distribution optimization, the classification difficulty of the extracted features notably decreases. Although some confusion persists among features corresponding to D7, T62, ZSU234, and ZIL131, features of different classes roughly occupy distinct positions in space, allowing for better differentiation between most features. Moreover, the level of confusion between features of T72 and BMP2 decreases, and features corresponding to 2S1 and BRDM2 almost do not overlap with those of other classes. Consequently, the model

TABLE III

Average Recognition Accuracy and PD rate of each Algorithm in the 1-way 5-shot Scenario

Algorithms	Recognition Accuracy (%) T^0	T^1	T^2	T^3	T^4	T^5	T^6	Average Accuracy (%)	PD rate (%)
iCaRL	99.45	72.69	77.66	65.90	58.48	53.58	52.09	68.55	47.36
ProtoNet	99.35	85.61	73.43	62.02	57.11	50.52	45.32	67.62	54.03
CEC	96.16	85.99	84.39	78.05	72.05	62.89	58.50	76.86	37.66
C-FSCIL	97.54	86.20	85.75	76.60	73.45	64.40	59.19	77.59	38.35
FACT	99.44	85.67	85.68	76.45	73.30	63.00	57.65	77.31	41.79
S3C	**99.70**	89.35	**92.46**	80.19	73.92	68.41	63.80	81.12	35.90
WaRP	98.83	88.24	85.27	77.26	73.51	64.02	59.05	78.03	39.78
ODF (ours)	99.69	**91.91**	89.24	**83.49**	**79.36**	**68.82**	**64.81**	**82.47**	**34.88**

TABLE IV

Average Recognition Accuracy and PD rate of each Algorithm in the 2-way 5-shot Scenario

Algorithms	Recognition Accuracy (%) T^0	T^1	T^2	T^3	Average Accuracy (%)	PD rate (%)
iCaRL	99.33	75.11	67.12	58.42	75.00	40.91
ProtoNet	99.41	76.38	60.06	47.88	70.93	51.53
CEC	96.77	84.39	72.87	59.75	78.45	37.02
C-FSCIL	97.25	86.21	75.06	61.32	79.96	35.93
FACT	99.32	85.77	73.11	59.69	79.47	39.63
S3C	**99.56**	88.74	71.30	60.70	80.08	38.86
WaRP	99.07	86.42	74.69	59.60	79.95	39.47
ODF (ours)	99.47	**89.65**	**77.50**	**65.97**	**83.15**	**33.50**

TABLE V

Average Recognition Accuracy and PD rate of each Algorithm in the 1-step 5-shot Scenario

Algorithms	Recognition Accuracy (%) T^0	T^1	Average Accuracy (%)	PD rate (%)
iCaRL	99.16	68.36	83.76	30.80
ProtoNet	99.16	68.36	83.76	30.80
CEC	96.68	60.42	78.55	36.26
C-FSCIL	95.79	62.85	79.32	32.94
FACT	98.94	64.07	81.51	34.87
S3C	**99.54**	68.46	84.00	31.08
WaRP	98.72	64.59	81.66	34.13
ODF (ours)	99.13	**69.20**	**84.17**	**29.93**

TABLE VI

Recognition Accuracy of the Model using Parameter Fine-tuning and Feature Orthogonal Distribution Optimization in the 1-way 5-shot Scenario

Methods	Recognition Accuracy (%) T^0	T^1	T^2	T^3	T^4	T^5	T^6
Parameter Fine-tune	98.78	84.39	77.05	69.58	64.01	55.62	50.45
Orthogonal Distribution Optimization	99.69	91.91	89.24	83.49	79.36	68.82	64.81

TABLE VII

Recognition Accuracy of the Model using Parameter Fine-tuning and Feature Orthogonal Distribution Optimization in the 2-way 5-shot and 1-step 5-shot Scenario

Methods	Recognition Accuracy (%) 2-way 5-shot scenario T^0	T^1	T^2	T^3	1-step 5-shot scenario T^0	T^1
Parameter Fine-tune	98.97	84.70	70.82	56.38	98.04	57.19
Orthogonal Distribution Optimization	99.47	89.65	77.50	65.97	99.13	69.20

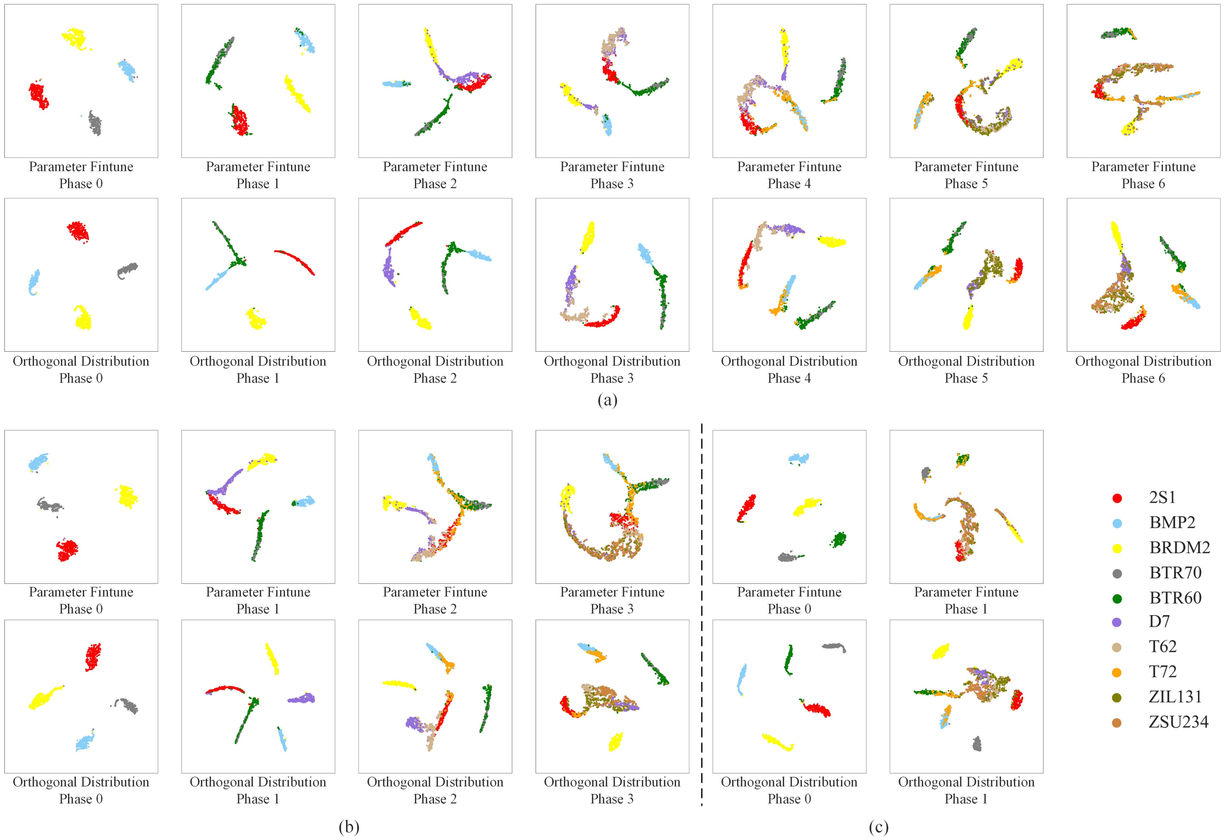

Fig. 7. The t-SNE Visualization Illustrating the Features Extracted by the Model using Parameter Fine-tuning and Feature Orthogonal Distribution Optimization. (a) 1-way 5-shot scenario. (b) 2-way 5-shot scenario. (c) 1-step 5-shot scenario.

achieves significantly higher recognition accuracy when utilizing feature orthogonal distribution optimization compared to parameter fine-tuning. In 2-way 5-shot and 1-step 5-shot scenarios, the advantages of feature orthogonal distribution optimization over parameter fine-tuning are similar to those observed in the 1-way 5-shot scenario. In conclusion, feature orthogonal distribution optimization proves effective in enhancing the spatial distribution of features under few-shot conditions. It improves the distinguishability of features among different classes, thereby improving target recognition performance.

Fig. 8 depicts the incremental recognition accuracy of the model under three conditions: without any augmentation, with image augmentation, and with high-dimensional feature random augmentation. The employed image augmentation techniques include several common methods: random cropping and scaling, random rotation, and random flipping. Compared to not using any augmentation, the model's recognition accuracy actually decreases when image augmentation is applied. We attribute this primarily to the difference in imaging principles between SAR and optical imaging. The distribution of scattering centers and the positions of shadows in the enhanced SAR images are inconsistent with real SAR images, which makes them unrepresentative of real SAR images, thereby misleading the neural network. On the contrary, high-dimensional feature random augmentation notably enhances the model's recognition performance across each incremental learning stage in the 1-way 5-shot scenario. Similar improvements of recognition accuracy can also be observed in the 2-way 5-shot and 1-step 5-shot scenarios. After learning all 10 classes, compared to not using any augmentation, the model's recognition accuracy increases by 0.96%, 1.66%, and 0.66% in the 1-way 5-shot, 2-way 5-shot, and 1-step 5-shot scenarios, respectively. The process of high-dimensional feature random augmentation is based on the characteristic that neural networks project images of the same class close to each other in the feature space. Thus, pseudo-features generated around real high-dimensional features serve to maintain the feature distribution of previously learned classes and complement the distribution of new-class features. This not only supplements the training samples for the dimensionality reduction layer, reducing the impact of overfitting, but also assists the dimensionality reduction layer in better projecting high-dimensional features from different classes onto the predefined orthogonal directions. In summary, random augmentation of high-dimensional features further strengthens the boundaries between features of different classes, leading to an overall improvement in recognition accuracy.

Tables VIII and IX present the few-shot incremental recognition results of the model using Euclidean distance criterion, cosine distance criterion, and joint decision criterion in three scenarios. The recognition accuracy under the Euclidean and cosine distance criteria is similar

TABLE VIII
Few-Shot Incremental Recognition Accuracy under Different Decision Criteria in the 1-way 5-shot Scenario

Methods	Recognition Accuracy (%)						
	T^0	T^1	T^2	T^3	T^4	T^5	T^6
Euclidean	99.53	91.64	89.53	80.71	76.00	68.36	63.33
Cosine	99.52	89.99	87.22	81.26	77.09	68.56	63.40
Joint Decision	99.69	91.91	89.24	83.49	79.36	68.82	64.81

TABLE IX
Few-Shot Incremental Recognition Accuracy under Different Decision Criteria in the 2-way 5-shot and 1-step 5-shot Scenario

Methods	Recognition Accuracy (%)					
	2-way 5-shot scenario				1-step 5-shot scenario	
	T^0	T^1	T^2	T^3	T^0	T^1
Euclidean	99.31	87.79	76.75	65.19	98.81	68.12
Cosine	99.66	90.03	77.27	65.33	99.09	67.87
Joint Decision	99.47	89.65	77.50	65.97	99.13	69.20

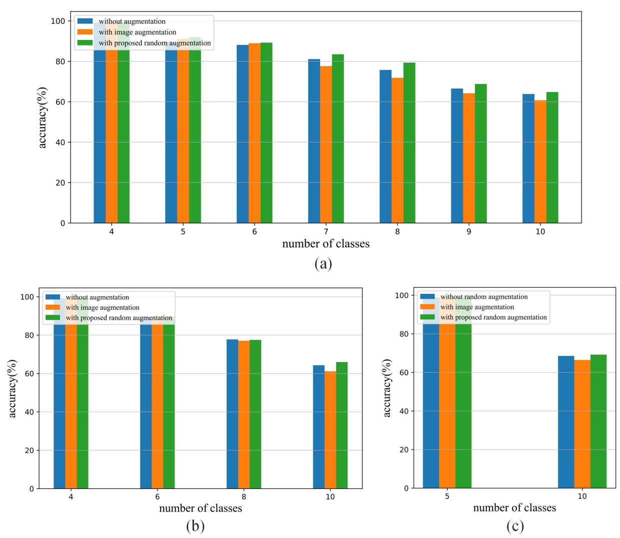

Fig. 8. Comparison of Recognition Accuracy when using different Augmentation Methods. (a) 1-way 5-shot scenario. (b) 2-way 5-shot scenario. (c) 1-step 5-shot scenario.

and both are lower than that under the joint decision criterion. In the 1-way 5-shot, 2-way 5-shot, and 1-step 5-shot scenarios, after the model learns targets of all 10 classes, the recognition accuracy using the joint decision criterion increases by 1.48%, 0.78%, and 1.08% compared to using the Euclidean distance criterion, and by 1.41%, 0.64%, and 1.33% compared to using the cosine distance criterion. Therefore, the joint decision criterion leverages the good separability characteristics of orthogonal distributed features under both Euclidean and cosine distance criteria, thereby providing more reasonable classification results compared to a single decision criterion and further improving target recognition accuracy.

D. Discussion

In this section, we discuss a range of parameters involved in the proposed method under the 1-way 5-shot scenario.

To analyze the impact of the number of pseudo-features generated around each real feature and the scale factor r of the random bias on recognition performance, we present the recognition accuracy of the model after learning all 10 classes with different values for these two parameters. As shown in Fig. 9, the optimal number of pseudo-features is 10, and the optimal value of the scale factor r is 2.5. When the number of pseudo-features is relatively small (e.g., 2 or 5), and the scale factor r is low (e.g., 1.0 or 2.0), the expansion of the feature space occupied by each class is insufficient. Pseudo-features fail to effectively simulate features of same-class samples that differ significantly from real high-dimensional features, thus limiting the improvement of the model's recognition performance. When the number of pseudo-features is too large (e.g., 20 or 50), the model may overly focus on pseudo-features and neglect real features, leading to a decrease in recognition accuracy. When the scale factor r is too large (e.g., 3.0, 5.0, or 10.0), the excessive random bias introduces incorrect information about the features' spacial distribution, misleading the model in establishing the classification boundaries for each class.

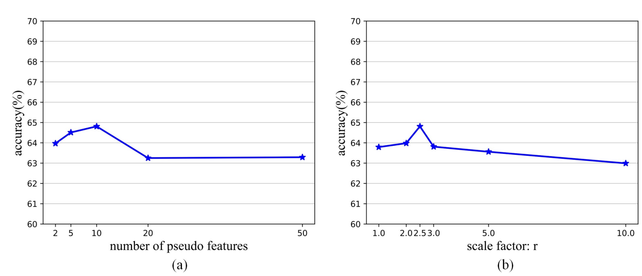

Fig. 9. Parameter Analysis of the High-Dimensional Feature Random Augmentation Process. (a) The Impact of Pseudo-Feature Quantity on Recognition Performance. (b) The Impact of Scale Factor on Recognition Performance.

Fig. 10 illustrates the recognition accuracy of the model after learning all 10 classes with different fixed values and adaptive values of the cosine distance weight coefficient a and the Euclidean distance weight coefficient b in the joint decision criterion. It is evident that the model achieves optimal target recognition accuracy when using adaptive coefficients. Fixing weight coefficients reduces the classifier's plasticity, leading to insufficient adaptability to dynamic tasks, which in turn limits the improvement of classification performance.

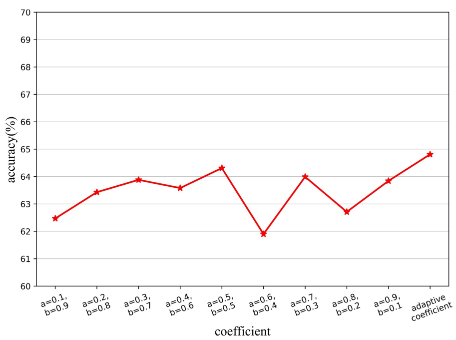

Fig. 10. Comparison of Fixed and Adaptive Coefficients in Joint Decision.

Additionally, we provide examples of adaptive coefficients during testing to more comprehensively analyze the joint decision criterion. As shown in Fig. 11, we consider that when $a > 0.8$, the decision is dominated by cosine distance, and when $b > 0.8$, it is dominated by Euclidean distance. The intermediate area represents a joint decision based on both distances. It is evident that most adaptive coefficients fall within the intermediate area, indicating that the classification decision is not overly dependent on a single distance. However, the adaptive coefficients also exhibit a tendency to favor Euclidean distance. This is because in joint decision criterion, the distance that can provide a clear judgment (i.e., the confidence for a particular class significantly exceeds that of others, rather than having multiple classes with similar confidence) is given a greater weight. Test samples that are less likely to be misclassified typically have features close to the prototypes, where both Euclidean and cosine distance criteria can provide clear judgments, resulting in weights with little differences for the two. Features that are easily confused with other classes typically deviate significantly from the prototype. The orthogonal distributed prototypes have the maximum margin of 90 degrees when measured by cosine distance, whereas there is no clear upper limit for the margin measured by Euclidean distance. Therefore, features near the boundary are more likely to obtain a clear judgment under the Euclidean distance criterion, leading to a bias towards Euclidean distance in the adaptive coefficients.

Finally, we compared the number of parameters and the floating point operations (FLOPs) required to infer a single image for our proposed ODF with the ResNet-18, which serves as the backbone. As shown in Table X, compared to ResNet-18, the ODF has only a slight

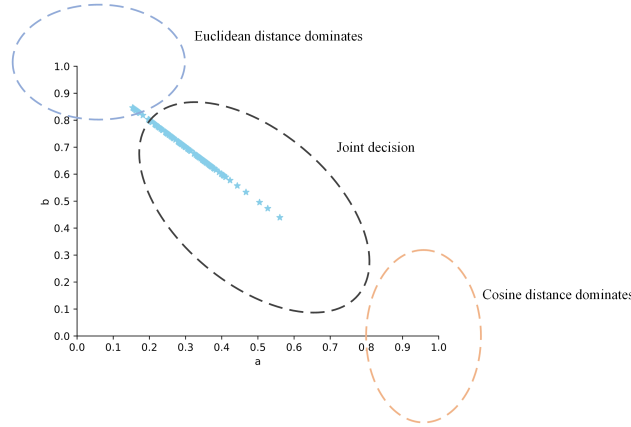

Fig. 11. Adaptive Coefficients Distribution.

increase in the number of parameters and FLOPs. The increase in the number of parameters is mainly due to the storage of high-dimensional features and prototypes of the previously learned classes, while the increase in FLOPs primarily comes from calculating the Euclidean and cosine distances between the feature of the test image and the prototypes of each class. In summary, the ODF does not significantly increase the model's storage and computational resource consumption.

TABLE X
Comparison of Model Parameter Size and Computational load

Models	Number of Parameters	FLOPs
ResNet-18	11.175M	142.442M
ODF	11.203M	142.470M

V. CONCLUSION

This paper introduces a SAR target few-shot incremental recognition approach based on orthogonal distribution features, with main contributions including feature orthogonal distribution optimization and random augmentation of high-dimensional features. Specifically, the orthogonal distribution optimization of features improves the features' spatial distribution during FSCIL process. This optimization strategy not only reduces mutual interference between features from different classes but also reserves space for features of new classes. The random augmentation method of high-dimensional features assists in strengthening the boundaries between features of different classes and alleviating overfitting issues in few-shot scenarios. Additionally, the joint decision criterion based on Euclidean and cosine distances effectively leverages the characteristics of orthogonal distributed features to make more reasonable classification decisions.

A series of SAR target few-shot incremental recognition experiments validate the effectiveness of the proposed algorithm. Compared with the existing FSCIL algorithms, ODF not only achieves the best target recognition accuracy but also demonstrates better adaptability to different few-shot incremental recognition scenarios. Therefore, ODF better meets the requirements of target recognition under sample deficiency conditions and has higher application value in complex and urgent scenarios such as emergency rescue.

Currently, ODF primarily improves the target recognition accuracy by optimizing the feature distribution in high-dimensional space, but it still underutilizes the scattering information of targets contained in SAR images. In the next step, we will incorporate the Attribute Scattering Center model and time-frequency analysis methods to embed the target scattering information into the deep learning framework. With the aid of scattering information, the model's performance in few-shot incremental recognition, as well as its generalization and interpretability, will be further enhanced.

REFERENCES

[1] F. Zhang, X. Sun, F. Ma, and Q. Yin, "Superpixelwise likelihood ratio test statistic for polsar data and its application to built-up area extraction," *ISPRS Journal of Photogrammetry and Remote Sensing*, vol. 209, pp. 233–248, 2024.

[2] Y. Li, X. Liang, and H. Jia, "Ship detection in sar images based on knowledge distillation," *Modern Defense Technology*, vol. 51, no. 4, p. 78, 2023.

[3] Z. Geng, H. Yan, J. Zhang, and D. Zhu, "Deep-learning for radar: A survey," *IEEE Access*, vol. 9, pp. 141 800–141 818, 2021.

[4] Z. Yue, F. Gao, Q. Xiong, J. Wang, T. Huang, E. Yang, and H. Zhou, "A novel semi-supervised convolutional neural network method for synthetic aperture radar image recognition," *Cognitive Computation*, vol. 13, pp. 795–806, 2021.

[5] Y. Zhou, H. Liu, F. Ma, Z. Pan, and F. Zhang, "A sidelobe-aware small ship detection network for synthetic aperture radar imagery," *IEEE Transactions on Geoscience and Remote Sensing*, vol. 61, pp. 1–16, 2023.

[6] F. Ma, X. Sun, F. Zhang, Y. Zhou, and H.-C. Li, "What catch your attention in sar images: Saliency detection based on soft-superpixel lacunarity cue," *IEEE Transactions on Geoscience and Remote Sensing*, vol. 61, pp. 1–17, 2023.

[7] Z. Li, F. Liu, W. Yang, S. Peng, and J. Zhou, "A survey of convolutional neural networks: analysis, applications, and prospects," *IEEE transactions on neural networks and learning systems*, 2021.

[8] Z. Mai, R. Li, J. Jeong, D. Quispe, H. Kim, and S. Sanner, "Online continual learning in image classification: An empirical survey," *Neurocomputing*, vol. 469, pp. 28–51, 2022.

[9] H. Huang, F. Gao, J. Sun, J. Wang, A. Hussain, and H. Zhou, "Novel category discovery without forgetting for automatic target recognition," *IEEE Journal of Selected Topics in Applied Earth Observations and Remote Sensing*, vol. 17, pp. 4408–4420, 2024.

[10] Z. Zheng, X. Nie, and B. Zhang, "Fine-grained continual learning for sar target recognition," in *IGARSS 2022-2022 IEEE International Geoscience and Remote Sensing Symposium*. IEEE, 2022, pp. 2207–2210.

[11] Y. Zhou, S. Zhang, X. Sun, F. Ma, and F. Zhang, "Sar target incremental recognition based on hybrid loss function and class-bias correction," *Applied Sciences*, vol. 12, no. 3, p. 1279, 2022.

[12] M. Masana, X. Liu, B. Twardowski, M. Menta, A. D. Bagdanov, and J. Van De Weijer, "Class-incremental learning: survey and performance evaluation on image classification," *IEEE Transactions on Pattern Analysis and Machine Intelligence*, vol. 45, no. 5, pp. 5513–5533, 2022.

[13] F. Gao, L. Kong, R. Lang, J. Sun, J. Wang, A. Hussain, and H. Zhou, "Sar target incremental recognition based on features with strong separability," *IEEE Transactions on Geoscience and Remote Sensing*, vol. 62, pp. 1–13, 2024.

[14] B. Li, Z. Cui, Z. Cao, and J. Yang, "Incremental learning based on anchored class centers for sar automatic target recognition," *IEEE Transactions on Geoscience and Remote Sensing*, vol. 60, pp. 1–13, 2022.

[15] J. Tang, D. Xiang, F. Zhang, F. Ma, Y. Zhou, and H. Li, "Incremental sar automatic target recognition with error correction and high plasticity," *IEEE Journal of Selected Topics in Applied Earth Observations and Remote Sensing*, vol. 15, pp. 1327–1339, 2022.

[16] S. Dang, Z. Cao, Z. Cui, Y. Pi, and N. Liu, "Class boundary exemplar selection based incremental learning for automatic target recognition," *IEEE Transactions on Geoscience and Remote Sensing*, vol. 58, no. 8, pp. 5782–5792, 2020.

[17] L. Wang, X. Yang, H. Tan, X. Bai, and F. Zhou, "Few-shot class-incremental sar target recognition based on hierarchical embedding and incremental evolutionary network," *IEEE Transactions on Geoscience and Remote Sensing*, vol. 61, pp. 1–11, 2023.

[18] Y. Zhao, L. Zhao, D. Ding, D. Hu, G. Kuang, and L. Liu, "Few-shot class-incremental sar target recognition via cosine prototype learning," *IEEE Transactions on Geoscience and Remote Sensing*, vol. 61, pp. 1–18, 2023.

[19] H. Huang, F. Gao, J. Wang, A. Hussain, and H. Zhou, "An incremental sar target recognition framework via memory-augmented weight alignment and enhancement discrimination," *IEEE Geoscience and Remote Sensing Letters*, vol. 20, pp. 1–5, 2023.

[20] S. Tian, L. Li, W. Li, H. Ran, X. Ning, and P. Tiwari, "A survey on few-shot class-incremental learning," *Neural Networks*, vol. 169, pp. 307–324, 2024.

[21] A. Kukleva, H. Kuehne, and B. Schiele, "Generalized and incremental few-shot learning by explicit learning and calibration without forgetting," in *Proceedings of the IEEE/CVF international conference on computer vision*, 2021, pp. 9020–9029.

[22] S. Dong, X. Hong, X. Tao, X. Chang, X. Wei, and Y. Gong, "Few-shot class-incremental learning via relation knowledge distillation," in *Proceedings of the AAAI Conference on Artificial Intelligence*, vol. 35, no. 2, 2021, pp. 1255–1263.

[23] A. Cheraghian, S. Rahman, P. Fang, S. K. Roy, L. Petersson, and M. Harandi, "Semantic-aware knowledge distillation for few-shot class-incremental learning," in *Proceedings of the IEEE/CVF conference on computer vision and pattern recognition*, 2021, pp. 2534–2543.

[24] Y. Tai, Y. Tan, S. Xiong, and J. Tian, "Mine-distill-prototypes for complete few-shot class-incremental learning in image classification," *IEEE Transactions on Geoscience and Remote Sensing*, vol. 61, pp. 1–13, 2023.

[25] Z. Song, Y. Zhao, Y. Shi, P. Peng, L. Yuan, and Y. Tian, "Learning with fantasy: Semantic-aware virtual contrastive constraint for few-shot class-incremental learning," in *Proceedings of the IEEE/CVF Conference on Computer Vision and Pattern Recognition*, 2023, pp. 24 183–24 192.

[26] G. Shi, J. Chen, W. Zhang, L.-M. Zhan, and X.-M. Wu, "Overcoming catastrophic forgetting in incremental few-shot learning by finding flat minima," *Advances in neural information processing systems*, vol. 34, pp. 6747–6761, 2021.

[27] D.-W. Zhou, F.-Y. Wang, H.-J. Ye, L. Ma, S. Pu, and D.-C. Zhan, "Forward compatible few-shot class-incremental learning," in *Proceedings of the IEEE/CVF conference on computer vision and pattern recognition*, 2022, pp. 9046–9056.

[28] H. Zhao, Y. Fu, M. Kang, Q. Tian, F. Wu, and X. Li, "Mgsvf: Multi-grained slow versus fast framework for few-shot class-incremental learning," *IEEE Transactions on Pattern Analysis and Machine Intelligence*, vol. 46, no. 3, pp. 1576–1588, 2024.

[29] A. F. Akyürek, E. Akyürek, D. T. Wijaya, and J. Andreas, "Subspace regularizers for few-shot class incremental learning," *arXiv preprint arXiv:2110.07059*, 2021.

[30] D.-Y. Kim, D.-J. Han, J. Seo, and J. Moon, "Warping the space: Weight space rotation for class-incremental few-shot learning," in *The Eleventh International Conference on Learning Representations, ICLR 2023, Kigali, Rwanda, May 1-5, 2023*. OpenReview.net, 2023, pp. 1–1. [Online]. Available: https://openreview.net/pdf?id=kPLzOfPfA2l

[31] B. Yang, M. Lin, B. Liu, M. Fu, C. Liu, R. Ji, and Q. Ye, "Learnable expansion-and-compression network for few-shot class-incremental learning," *arXiv preprint arXiv:2104.02281*, 2021.

[32] X. Tao, X. Hong, X. Chang, S. Dong, X. Wei, and Y. Gong, "Few-shot class-incremental learning," in *Proceedings of the IEEE/CVF Conference on Computer Vision and Pattern Recognition*, 2020, pp. 12 183–12 192.

[33] C. Zhang, N. Song, G. Lin, Y. Zheng, P. Pan, and Y. Xu, "Few-shot incremental learning with continually evolved classifiers," in *Proceedings of the IEEE/CVF conference on computer vision and pattern recognition*, 2021, pp. 12 455–12 464.

[34] B. Yang, M. Lin, Y. Zhang, B. Liu, X. Liang, R. Ji, and Q. Ye, "Dynamic support network for few-shot class incremental learning," *IEEE Transactions on Pattern Analysis and Machine Intelligence*, vol. 45, no. 3, pp. 2945–2951, 2022.

[35] J. Yoon, S. Madjid, S. J. Hwang, C.-D. Yoo *et al.*, "On the soft-subnetwork for few-shot class incremental learning," in *The Eleventh International Conference on Learning Representations, ICLR 2023, Kigali, Rwanda, May 1-5, 2023*. OpenReview.net, 2023, pp. 1–1. [Online]. Available: https://openreview.net/pdf?id=z57WK5lGeHd

[36] G. Zheng and A. Zhang, "Few-shot class-incremental learning with meta-learned class structures," in *2021 International Conference on Data Mining Workshops (ICDMW)*. IEEE, 2021, pp. 421–430.

[37] K. Zhu, Y. Cao, W. Zhai, J. Cheng, and Z.-J. Zha, "Self-promoted prototype refinement for few-shot class-incremental learning," in *Proceedings of the IEEE/CVF conference on computer vision and pattern recognition*, 2021, pp. 6801–6810.

[38] M. Hersche, G. Karunaratne, G. Cherubini, L. Benini, A. Sebastian, and A. Rahimi, "Constrained few-shot class-incremental learning," in *Proceedings of the IEEE/CVF Conference on Computer Vision and Pattern Recognition*, 2022, pp. 9057–9067.

[39] Y. Zou, S. Zhang, Y. Li, and R. Li, "Margin-based few-shot class-incremental learning with class-level overfitting mitigation," *Advances in neural information processing systems*, vol. 35, pp. 27 267–27 279, 2022.

[40] L. Zhang, X. Leng, S. Feng, X. Ma, K. Ji, G. Kuang, and L. Liu, "Domain knowledge powered two-stream deep network for few-shot sar vehicle recognition," *IEEE Transactions on Geoscience and Remote Sensing*, vol. 60, pp. 1–15, 2022.

[41] ——, "Azimuth-aware discriminative representation learning for semi-supervised few-shot sar vehicle recognition," *Remote Sensing*, vol. 15, no. 2, p. 331, 2023.

[42] M. Yang, X. Bai, L. Wang, and F. Zhou, "Henc: Hierarchical embedding network with center calibration for few-shot fine-grained sar target classification," *IEEE Transactions on Image Processing*, vol. 32, pp. 3324–3337, 2023.

[43] X. Bai, M. Yang, B. Chen, and F. Zhou, "Remi: Few-shot isar target classification via robust embedding and manifold inference," *IEEE Transactions on Neural Networks and Learning Systems*, pp. 1–14, 2024.

[44] Y. Zhao, L. Zhao, S. Zhang, K. Ji, G. Kuang, and L. Liu, "Azimuth-aware subspace classifier for few-shot class-incremental sar atr," *IEEE Transactions on Geoscience and Remote Sensing*, vol. 62, pp. 1–20, 2024.

[45] K. He, X. Zhang, S. Ren, and J. Sun, "Deep residual learning for image recognition," in *Proceedings of the IEEE conference on computer vision and pattern recognition*, 2016, pp. 770–778.

[46] E. R. Keydel, S. W. Lee, and J. T. Moore, "Mstar extended operating conditions: A tutorial," *Algorithms for Synthetic Aperture Radar Imagery III*, vol. 2757, pp. 228–242, 1996.

[47] A. Paszke, S. Gross, F. Massa, A. Lerer, J. Bradbury, G. Chanan, T. Killeen, Z. Lin, N. Gimelshein, L. Antiga *et al.*, "Pytorch: An imperative style, high-performance deep learning library," *Advances in neural information processing systems*, vol. 32, 2019.

[48] S.-A. Rebuffi, A. Kolesnikov, G. Sperl, and C. H. Lampert, "icarl: Incremental classifier and representation learning," in *Proceedings of the IEEE conference on Computer Vision and Pattern Recognition*, 2017, pp. 2001–2010.

[49] J. Snell, K. Swersky, and R. Zemel, "Prototypical networks for few-shot learning," *Advances in neural information processing systems*, vol. 30, 2017.

[50] J. Kalla and S. Biswas, "S3c: Self-supervised stochastic classifiers for few-shot class-incremental learning," in *European Conference on Computer Vision*. Springer, 2022, pp. 432–448.

[51] L. Van der Maaten and G. Hinton, "Visualizing data using t-sne." *Journal of machine learning research*, vol. 9, no. 11, 2008.

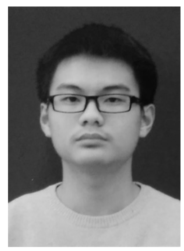

Lingzhe Kong received the B.S. degree in electronic and information engineering from Beihang University, Beijing, China, in 2021. He is currently pursuing the Ph.D. degree in information and communication engineering at Beihang University.

His current research activities are in target recognition and synthetic aperture radar image processing.

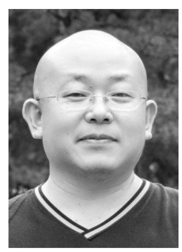

Fei Gao received the B.S. degree in industrial electrical automation, and the M.S. degree in electro-magnetic measurement technology and instrument from the Xi'an Petroleum Institute, Xi'an, China, in 1996 and 1999, respectively, and the Ph.D. degree in signal and information processing from the Beihang University, Beijing, China, in 2005.

He is currently a Professor with the School of Electronic and Information Engineering, Beihang University. His research interests include target detection and recognition, image processing, deep learning for applications in remote sensing.

Xiaoyu He Xiaoyu He was born in Jiangxi, China, in 1991. He received the B.S. degree from the School of Mechanical and Electric Engineering, Guangzhou University, Guangzhou, China, in 2012, and the Ph.D. degree in signal and information processing from the School of Electronics and Information Engineering, Beihang University, Beijing, China, in 2018.

He is currently a Lecturer with the School of Electronics and Information Engineering, Beihang University, where he was mainly involved in research of characteristic modeling for multispectral and hyperspectral imagery, radar system modeling, and signal processing.

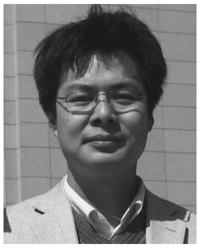

Jun Wang received the B.S. degree in communication engineering from the North western Polytechnical University, Xi'an, China, in 1995 and the M.S.and Ph.D. degrees in signal and information processing from the Beijing University of Aeronautics and Astronautics (BUAA), Beijing, China, in 1998 and2001, respectively.

He is currently a Professor with the School of Electronic and Information Engineering, BUAA. He is interested in signal processing, DSP/FPGA real time architecture, target recognition and tracking, and so on. His research has resulted in over 40 papers in journals, books, and conference proceedings.

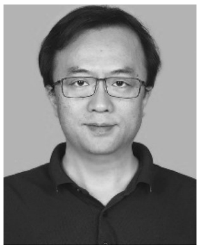

Jinping Sun (Member, IEEE) received the M.Sc. and Ph.D. degrees from Beihang University (BUAA), Beijing, China, in 1998 and 2001, respectively.

He is currently a Professor with the School of Electronic and Information Engineering, BUAA. His research interests include statistical signal processing, high-resolution radar signal processing, target tracking, image understanding, and robust beamforming.

Huiyu Zhou received the B.Eng. degree in radio technology from Huazhong University of Science and Technology, Wuhan, China, the M.S. degree in biomedical engineering from University of Dundee,Dundee, U.K., and the Doctor of Philosophy degree in computer vision from Heriot-Watt University,Edinburgh, U.K.

He is currently a Professor with the School of Informatics, University of Leicester, Leicester, U.K.He has published widely in medical image processing, computer vision, intelligent systems, and data mining.

Amir Hussain received the B.Eng. (Hons.) and Ph.D. degrees from the University of Strathclyde, Glasgow, U.K., in 1992 and 1997, respectively.

He is Founding Director of the Centre of AI and Robotics at Edinburgh Napier University, U.K. He has led major national and international projects and supervised over 40 Ph.D. students. He has authored several patents and over 600 publications, including around 300 journal papers and20 Books/monographs. His research interests are cross-disciplinary and industry-led, and aimed at developing responsible AI and cognitive data science technologies to engineer the smart healthcare and industrial systems of tomorrow.

Dr. Hussain is Founding Chief Editor of Springer's Cognitive Computation journal and invited Editor for various other journals. Amongst other distinguished roles, he has served as General Chair of the flagship 2020 IEEE World Congress on Computational Intelligence (WCCI) and the 2023 IEEE Smart World Congress (SWC). He is Chair of the IEEE U.K. and Ireland Chapter of the IEEE Industry Applications Society.